Journal of Controlled Release 318 (2020) 185–196

Contents lists available at ScienceDirect

Journal of Controlled Release

journal homepage: www.elsevier.com/locate/jconrel

Development of hydrogel-like biomaterials via nanoparticle assembly and solid-hydrogel transformation

James Coyne, Nan Zhao, Anuoluwapo Olubode, Mridula Menon, Yong Wang*

Department of Biomedical Engineering, The Pennsylvania State University, University Park, PA 16802, USA

ARTICLE INFO

Keywords:
Nanoparticle assembly
Solid-gel transformation
Growth factor delivery
Aptamer
Regenerative medicine

ABSTRACT

Hydrogels for biomedical applications such as controlled drug release are usually synthesized with the chemical or physical crosslinking of monomers or macromers. In this work, we used gelatin to prepare hydrogel nanoparticles and studied whether gelatin nanoparticles (GNPs) could assemble to form a solid biomaterial and whether this solid biomaterial was capable of transforming into a hydrogel upon introduction to a hydrated environment. The data show that GNPs with or without aptamer functionalization could form a nanoparticle-assembled porous solid biomaterial after freezing and lyophilization treatment. This formation did not need any additional crosslinking reactions. More importantly, this solid biomaterial could undergo solid-to-hydrogel transition after contacting a solution and this transformation was tunable to match different shapes and geometries of defined molds. The formed hydrogel could also sequester and release growth factors for the promotion of skin wound healing. Thus, GNP-assembled solid biomaterials hold great potential as an off-the-shelf therapy for biomedical application such as drug delivery and regenerative medicine.

1. Introduction

Hydrogels are networks of hydrophilic polymer chains with large amounts of water [1]. They have been widely studied for biomedical applications such as drug delivery and regenerative medicine since they can slowly release biomolecules to elicit specific cellular responses [2–6]. However, it is challenging to develop hydrogels into off-the-shelf biomaterials loaded with biomolecules because of their intrinsic nature of containing water. Moreover, biomolecules such as proteins in an aqueous environment can easily lose their bioactivity if stored on the shelf [7–10]. Thus, it would be ideal that a pre-existing solid-like biomaterial in a dry form can be synthesized and ready for transformation into a hydrogel once contacting and sequestering a drug solution. This kind of biomaterial can be stored on the shelf. It also possesses certain properties (e.g., containing water) of hydrogels for an application. The purpose of this work was to explore a biomaterial that can transform from a solid foam to a hydrogel-like biomaterial capable of sequestering and releasing proteins.

Hydrogels can be synthesized with numerous methods. A commonly used method is the chemical crosslinking of monomers to form covalently crosslinked hydrogels during a reaction. For instance, acrylamide subunits are chemically crosslinked to form polyacrylamide hydrogels through free radical polymerization [11]. Hydrogels can also be synthesized through physical crosslinking via hydrogen bonding, electrostatic attraction and/or hydrophobic association [12]. For example, polymers in the temperature-responsive poloxamer solutions can aggregate to form hydrogels via the dehydration of the hydrophobic units and the procedure of micellization when the solutions reach a situation above the critical micelle temperature and critical micelle concentration [13]. In this work, we integrated chemical and physical crosslinking mechanisms to develop a solid-like foam using the physical assembly of chemically crosslinked hydrogel nanoparticles.

Gelatin is a natural polymer derived from collagen. It has been used to develop various bulk hydrogels for controlled protein release [14]. Gelatin has also been used to synthesize hydrogel nanoparticles [15–18]. All of these gelatin-based bulk hydrogels or hydrogel nanoparticles were synthesized through the chemical crosslinking of gelatin macromers. Differently, we developed a foam-like solid biomaterial using gelatin in two steps. We first synthesized gelatin nanoparticles by using a precipitation-crosslinking method and then lyophilized nanoparticle suspension to prepare the foam-like biomaterial through physical nanoparticle assembly. The foam-like solid biomaterial and its transformation into a hydrogel were characterized through imaging techniques. Its capability of sequestering and releasing proteins was examined using vascular endothelial growth factor (VEGF) as a model. Moreover, this material was used to treat skin wound for evaluating its

* Corresponding author.
E-mail address: yxw30@psu.edu (Y. Wang).

https://doi.org/10.1016/j.jconrel.2019.12.026
Received 30 October 2019; Received in revised form 7 December 2019; Accepted 15 December 2019
Available online 16 December 2019

potential of releasing proteins for tissue regeneration.

2. Materials and methods

2.1. Materials

2.1.1. Chemical reagents

Gelatin (porcine, type A, 300 bloom), glutaraldehyde (25% in H_2O), acetone, dimethyl sulfoxide (DMSO), tween-20, ammonium persulfate, tetramethylethylenediamine (TEMED), sodium hydroxide, hydrochloric acid, and sodium citrate were obtained from Sigma Aldrich (St. Louis, MO). Dibenzocyclooctyne (DBCO)-PEG_4-NHS ester was obtained from Click Chemistry Tools (Scottsdale, AZ). Phosphate buffered saline (PBS), Dulbecco's phosphate buffered saline (DPBS), (5-(and-6)-carboxyfluorescein succinimidyl ester (5(6)-FAM SE), glycerol, sodium bicarbonate and acrylamide/bisacrylamide were obtained from Thermo-Fisher Scientific (Waltham, MA).

2.1.2. Biological reagents

Calcein AM, glycine, bovine serum albumin (BSA), fetal bovine serum (FBS), medium 200 (M200), medium 106 (M106), medium 154 (M154), Low Serum Growth Supplement (LSGS), ABTS substrate, xylene substitute mountant, ProLong Diamond Antifade Mountant with DAPI, goat anti-rabbit IgG-Alexa Fluor 546 antibody, α-smooth muscle actin antibody-Alexa Fluor 488 antibody (α-SMA), and Human umbilical vein endothelial cells (HUVECs), were obtained from ThermoFisher Scientific. Nucleic acid sequences were obtained from Integrated DNA Technologies (Coralville, IA). Vascular endothelial growth factor-165 (VEGF) and VEGF enzyme-linked immunosorbent assay (ELISA) kit were obtained from Peprotech (Rocky Hill, NJ). 4% Paraformaldehyde was obtained from Santa Cruz (Dallas, TX). Primary rabbit anti-mouse CD31 antibody was obtained from Cell Signaling Technology (Beverly, MA). Human neonatal fibroblasts (HDFN) and mouse keratinocytes (MK) were obtained from ATCC (Manassas, VA). Hematoxylin and eosin (H&E) stain kit was obtained from Leica Biosystems (Buffalo Grove, IL). Collagenase P. was obtained from Sigma Aldrich (St. Louis, MO).

2.1.3. Other materials

Tegaderm was obtained from 3 M Health Care (St. Paul, MN). Hair depilatory cream was obtained from VEET (UK).

2.2. Preparation of gelatin nanoparticles

GNPs were prepared using a previously described two-step desolvation method with slight modifications [15,16,18]. Gelatin (500 mg) was dissolved in 10 mL of DI water by heating to 50 °C for 10 min. While the solution was stirred at 250 rpm, 10 mL of acetone was added to precipitate high molecular weight gelatin. After removing the supernatant, containing the low molecular weight gelatin, the precipitated high molecular weight gelatin was re-dissolved in water by heating to 50 °C for 10 min. The dissolved gelatin was cooled to room temperature and the pH was adjusted to 2. Then 35 mL of acetone was slowly added dropwise to the solution to precipitate GNPs. The solution containing the precipitated GNPs was composed of a 30/70 water/acetone mixture. After acetone addition, 0.2 mL glutaraldehyde (25%) was added to the solution and it was incubated for 12 h to crosslink the nanoparticles. To block any unreacted aldehyde groups, 5 mL of glycine (100 mM) was added and the solution was incubated for 1 h. The particles were isolated by centrifugation at 9600 *g* for 20 min and washed three times with 70% acetone. After the final wash, the nanoparticles were re-suspended in DI water and the pH of the solution was adjusted to 7 using NaOH (0.1 M). The nanoparticles were stored at 4 °C until further use.

2.3. Characterization of GNPs

Dynamic light scattering (DLS, Zetasizer Nano-S, Malvern Instruments Ltd.) was used to measure the GNPs' size and charge. The nanoparticles were dispersed in water to a final concentration of 0.1 mg/mL and then characterized. The morphology of the GNPs was observed by first sputter coating with iridium and then imaging using a field emission scanning electron microscopy (Nova NanoSEM, 630, FEI, USA).

2.4. Assembly of GNPs

GNPs were dispersed in PBS to a final concentration of 5 mg/mL. 0.2 mL of the solution was transferred to a disc mold and frozen at −80 °C for 30 min. The frozen samples were lyophilized in a Labconco FreeZone 4.5^+ (Kansas City, MO) overnight. After lyophilization, the GNP-assembled biomaterial was placed in a sterile 24-well plate and stored at room temperature (RT) until further use. The morphology of the GNP assembly in the dry state was characterized by first sputter coating with iridium and imaged using a field emission scanning electron microscope (FESEM; Apreo, FEI, USA). Bright-field images of the dry and hydrated GNP-assembled biomaterial were obtained using a Nikon SMZ745T microscope (Tokyo, Japan).

2.5. Preparation of fluorescent GNPs

Fluorescent GNPs were prepared by first dissolving 5(6)-FAM SE (2 mg) in 200 μL of DMSO to a final concentration of 10 mg/mL. 15 μL of the 5(6)-FAM SE solution was added to GNP (1 mg) dissolved in sodium bicarbonate (0.1 M). The reaction mixture was incubated at 25 °C for 12 h. The unreacted reagents were removed using a dialysis cassette (MWCO = 20 kDa) in DI water for three days. The FAM-labeled GNPs (GNP-FAM) were observed using an Olympus IX73 microscope (Center Valley, PA) to ensure the particles were fluorescently labeled.

2.6. Assembly of FAM-labeled GNPs

200 μL of the GNP-FAM solution (5 mg/mL) was added to a glass surface and a glass coverslip was placed on top of the solution. Fluorescent images were taken using an Olympus IX73 microscope (IX73) after the deposition of the solution, after the particles were frozen at −80 °C for 30 min and then thawed, and after the particles were frozen at −80 °C for 30 min then lyophilized.

GNPs with and without FAM-labeling were dissolved in PBS at a final GNP concentration of 5 mg/mL and a final GNP-FAM concentration of 0.05 mg/mL. 0.2 mL of the solution was transferred to a disc mold and frozen at −80 °C for 30 min. The frozen samples were lyophilized in the Labconco FreeZone 4.5^+ (Kansas City, MO) instrument overnight. After lyophilization, the GNP-assembled biomaterial was placed in a 24-well plate and stored at RT until further use.

2.7. Characterization of the GNP-assembled biomaterial

The three-dimensional structure of the GNP-assembled biomaterial, dried and hydrated, was characterized by imaging with a confocal microscope (Olympus FV1000, Center Valley, PA). The images were used to quantify the void space in the dry and hydrated biomaterials by using ImageJ to determine the number of fluorescent pixels and subtracting this value from the total pixel area of the image. The difference was normalized by the total area to determine the void space percentage.

The change in thickness of the material during the transition from a sponge-like biomaterial to a hydrogel was determined by securing the material to a microscope slide and imaged using a Maestro imaging system (CRI, Woburn, MA). 10 μL of PBS was added to induce the

transition to a hydrogel and imaged again. ImageJ was used to measure the thickness.

The ability of the dry disc-like material to conform to different geometries after hydration was assessed by applying the GNP-assembled biomaterial to a triangular, circular, or square mold containing 10 μL of PBS. The molds were 3D printed using a Formlabs Form 2 (Somerville, MA). Bright-field images of the hydrogels were taken using a digital camera.

2.8. Preparation of aptamer-functionalized gelatin nanoparticles (aGNPs)

GNPs (500 mg) were reacted with DBCO-PEG_4-NHS (300 μM) to synthesize nanoparticles modified with DBCO. The unreacted reagents were removed using a dialysis cassette (MWCO = 20 kDa) in DI water for three days. Azide-modified anti-VEGF aptamer (100 pmol) was mixed with 140 μg of the DBCO-functionalized GNPs and incubated at 25 °C for 4 h.

2.9. Characterization of aGNPs

Polyacrylamide gel electrophoresis (PAGE) was used to determine the conjugation of aptamer to DBCO-modified nanoparticles. 4 μL of the aGNP (~10 pmol of aptamer) solution was incubated with 2 μL of Cy5-labeled complementary DNA sequence (100 μM) for 30 min at 25 °C. The mixture was added to a polyacrylamide gel (10 *w/v*%). After running the gel at 80 V for 40 min, a Maestro imaging system (CRI, Woburn, MA) was used to image and quantify the fluorescent intensity of the bands. Free anti-VEGF aptamer (10 pmol) incubated with Cy5-labeled complementary sequence was used as control. Dynamic light scattering (DLS, Zetasizer Nano-S, Malvern Instruments Ltd.) was used to measure the aGNPs' size and charge. The nanoparticles were dispersed in water to a final concentration of 0.1 mg/mL and then characterized. GNPs dispersed in water to a final concentration of 0.1 mg/mL were used as control.

2.10. Assembly of GNPs

GNPs with or without aptamer (0.7 pmol aptamer/μg GNP) were dissolved in PBS at a final nanoparticle concentration of 5 mg/mL and a final aptamer concentration of 0.5 μM. 0.2 mL of the solution was transferred to a disc mold and frozen at −80 °C for 30 min. The frozen samples were lyophilized in the Labconco FreeZone 4.5^+ (Kansas City, MO) instrument overnight. After lyophilization, the aGNP-assembled biomaterial was placed in a 24-well plate and stored at RT until used.

2.11. VEGF retention and release

2.11.1. VEGF retention

aGNP-assembled biomaterials with a final anti-VEGF aptamer concentration of 0.5 μM were synthesized to determine if the presence of aptamer would enable the retention of VEGF. To the dry biomaterial, VEGF (200 ng) was added and the VEGF-loaded hydrogels were immediately immersed in 0.5 mL of release media (0.1% BSA in PBS or M200). After 24 h, the release media was collected and analyzed using an enzyme-linked immunosorbent assay (ELISA) according to the protocol provided by the manufacturer. GNP-assembled biomaterials without aptamer were loaded with VEGF (200 ng) and used as control. The total VEGF amount remaining in the material was determined by incubation with anti-VEGF complementary sequence (100 pmol) and digestion with Collagenase P. (1 mg/mL).

2.11.2. VEGF release

To assess the sustained release of VEGF from the biomaterials, VEGF (200 ng) was added to the aGNP-assembled biomaterial containing anti-VEGF aptamer (100 pmol). The gels were incubated in 0.5 mL release media. At predetermined time points, 0.5 mL of the media was collected and replaced with fresh media. After the media was collected on day 10, the material was incubated with anti-VEGF complementary sequence (100 pmol) and digested with Collagenase P. (1 mg/mL) The collected release media were stored at −20 °C until analysis. The amount of VEGF was quantified using ELISA after all of the samples were collected. The data were presented as a cumulative release.

2.12. Cell culture

HDFNs were expanded using M106 supplemented with 10% FBS in 0.1% gelatin-coated cell culture flasks. HUVECs were expanded using M200 supplemented with 2% low serum growth supplement in 0.1% gelatin-coated cell culture flasks. MKs were expanded using M154 supplemented with 10% FBS in cell culture flasks. Cells of passage 6–10 were used in all cell experiments.

2.13. Tube formation assay

The bioactivity of the released VEGF was measured by the human umbilical vein endothelial cell (HUVEC) tube formation assay conducted according to previously established methods [19]. Briefly, 80 μL of the thawed Geltrex was added to a 48-well plate and incubated for 30 min at 37 °C. The day 10 release media from the in vitro VEGF release study was used for this study. The release media from the aGNP hydrogel (Apt (+)) was diluted to a final VEGF concentration of 10 ng/mL. The release media from the GNP hydrogel (Apt (−)) was used without further dilution (VEGF: 0.4 ng/mL). 200 μL of the different release media were added to the Geltrex coated cells after seeding with 4×10^4 HUVECs. 200 μL of stock VEGF at a concentration of 10 ng/mL was used as a control. After incubation at 37 °C for 4 h, the cells were stained with Calcein AM (2 μg/mL) for 30 min. The cells were imaged using the Olympus IX73 microscope (Center Valley, PA) and the total tube length was measured using ImageJ.

2.14. Cell proliferation on GNP-assembled biomaterials

Cells (HUVECs, HDFNs, or MKs) were seeded at a density of 1×10^4 cells per well on the aGNP-assembled biomaterial without VEGF (aGNP), aGNP-assembled biomaterial loaded with 100 ng of VEGF (aGNP- VEGF), or a GNP-assembled biomaterial loaded with a 100 ng of VEGF (GNP-VEGF). At days 1 and 7, the cells were stained with Calcein AM and imaged. The number of cells on the hydrogel were quantified using ImageJ.

2.15. Wound healing assay

All animal experiments were performed according to a protocol approved by the Pennsylvania State University Institutional Animal Care and Use Committee. Balb/c mice (age of 9–11 weeks) with weight 20–25 g were used. Avertin (1.2%) and ketoprofen (1 mg/mL) were injected intraperitoneally into the mice, 20 μL/g and 10 μL/g respectively. The dorsal hair of the mice was removed by an electric razor followed by application of Veet hair depilatory cream. The depilatory cream was cleaned by washing with sterile DPBS. The following day, the skin was sterilized with povidone-iodine and 70% ethanol. Two 6 mm circular full skin wounds were created on the dorsal skin. After the materials were applied, 12 mm × 12 mm Tegaderm film was applied to prevent wound contraction [20]. aGNP, GNP-VEGF (VEGF: 200 ng), and aGNP- VEGF (VEGF: 200 ng) biomaterials were used to treat the wounds. Tegaderm film alone was used as control. At different days, optical images of the wounds were taken using a digital camera.

2.16. Histological analysis

Mice were euthanized at day 10 and the wound sites on the skin were collected with a 6 mm biopsy punch. The tissue samples were cut

in half at the center of the wound. Both halves were embedded in paraffin and sectioned into 5 μm tissue sections. Tissue sections were stained with hematoxylin and eosin (H&E) in a Leica autostainer (Buffalo Grove, IL). The distance between the wound margins and the epithelial tongues were measured using ImageJ. The epithelization ratio was calculated by dividing the length of the epithelial layer by the initial length of the wound.

2.17. Immunostaining

The tissue sections were immunostained using a previously established method [21]. Paraffin-blocked tissue sections (5 μm) were deparaffinized and boiled in sodium citrate buffer (pH = 6) for 20 min. The sections were cooled to room temperature and washed with PBS. The sections were blocked with serum-blocking solution (3% BSA and 3% goat serum in PBS) for 1 h at RT. The tissue was washed and then incubated with rabbit anti-mouse CD31 antibody (1:200 dilution) overnight at 4 °C. After removal of unbound antibody, the tissues were incubated with goat anti-rabbit IgG-Alexa Fluor 546 secondary antibody (1:200 dilution) for 2 h at RT. The tissues were washed and incubated with fluorescent-labeled α-SMA antibody (1:200 dilution) overnight at 4 °C. After washing, the samples were mounted with ProLong Diamond Antifade Mountant with DAPI. The fluorescent images of the samples were taken with the Olympus IX73 (Center Valley, PA) microscope. The total number of blood vessels and blood vessel area was quantified using ImageJ. The $CD31^+$ blood vessels and blood vessels with both $CD31^+$ and α-SMA are shown.

2.18. Statistics

Prism 5.0 (Graphpad Software Inc., La Jolla) was used for all statistical analysis. All the data were presented as mean ± standard deviation, unless specified otherwise. One-way analysis of variance (ANOVA) with the Bonferroni post-test was performed to compare multiple groups. Unpaired Student's t-test was performed for the comparison of two groups. The data was considered statistically significant when p-value $\leq .05$.

3. Results and discussion

3.1. Synthesis of GNP-assembled biomaterials

Gelatin has been used to develop various biomaterials at both bulk and nanoscale levels for its biocompatibility and biodegradability [22–24]. Thus, we used gelatin to prepare nanoparticles in this work. The methods and major steps for preparing GNPs and using the GNPs as building blocks to develop bulk biomaterials are schematically illustrated in Fig. 1. GNPs were produced via a two-step desolvation method and then chemically crosslinked [15–17]. The nanoparticles were approximately 300 nm in diameter (Fig. 2A). It had a zeta potential of +11.4 mV (Fig. 2A), which suggests that the nanoparticles were positively charged. After the synthesis of the nanoparticles, we applied freezing and lyophilization to treat the suspension of nanoparticles in a disc mold. This treatment led to the formation of an integrated solid bulk biomaterial (Fig. 2B). With the aid of SEM imaging, we found that the biomaterials had macroporous structures. The image of the non-porous regions indicates that nanoparticles aggregated and fused together. It suggests that the nanoparticles suspended in an aqueous solution could be automatically assembled to form macroporous sponge-like structures during the procedure of lyophilization.

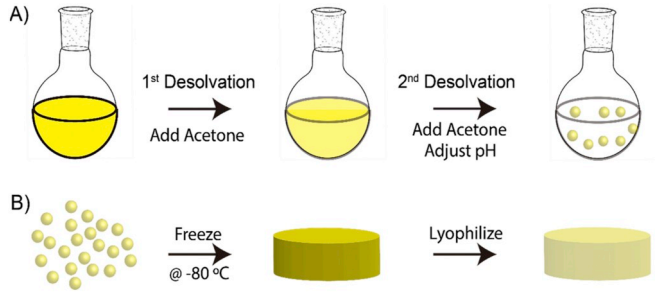

Fig. 1. Schematic illustration. A) Preparation of gelatin nanoparticles (GNPs) via a two-step desolvation method. Gelatin is precipitated using acetone. In the second step, pH is adjusted to 2 before the dropwise addition of acetone and glutaraldehyde. B) Preparation of GNP-based biomaterials via freezing and lyophilization that are performed sequentially. After the process of freezing and lyophilizing GNPs, a dry foam-like biomaterial is obtained.

After this biomaterial was treated with water, it absorbed water and formed a soft hydrogel that could maintain its stability in a gentle shaking condition (Fig. S1) and also be picked up using a tweezer (Fig. 2B). We also characterized the rheological properties of the hydrogel. The rheology data demonstrated that the storage (G') and loss modulus (G") of the hydrogel were 5800 Pa and 250 Pa, respectively (Fig. S2). Notably, when the same hydration procedure was applied to treat lyophilized gelatin, the material was dissolved rather than transitioning to a soft hydrogel (Fig. S3). To further determine whether the hydrogel structure was attributed to GNP assembly, the biomaterial was treated with Collagenase P. The hydrogels were quickly degraded (Fig. S4). It suggests that the hydrogels are biodegradable. Moreover, in comparison to the stability of the hydrogels in the enzyme-free solution (Fig. S1), the data further suggests that the physical crosslinking of the GNPs produced the hydrogel.

To ensure that this observation was not an artifact, we compared three nanoparticle systems (Fig. 3A) including the suspension of GNPs without any treatment, the suspension of GNPs that were frozen at −80 °C and subsequently thawed, and the suspension of GNPs that were frozen and lyophilized. For clear observation, we put those suspensions on the glass surface and covered with a glass coverslip. The results demonstrate that the normal suspension of GNPs was stable and the nanoparticles were well-dispersed without forming obvious aggregates even though the suspension was stored on the bench for several days or weeks. Similarly, freezing at −80 °C and thawing afterwards at room temperature did not induce significant nanoparticle aggregation. By contrast, the combination of freezing and lyophilization reproducibly induced the aggregation of GNPs. Under the coverslip, the aggregated nanoparticles formed thread or bundle-like structures.

Previous studies have shown that nanoparticles have a tendency to form aggregates or clusters up to several microns in size [25–29]. This aggregation happens when a physical process brings nanoparticles to a short distance and short-range thermodynamic interactions facilitate nanoparticle-nanoparticle attachment [30]. Electric-double-layer potentials and van der Waals determine if forces between nanoparticles are net attractive or repulsive for them to stick together [31–33]. During the normal storage or freezing procedure, the concentration of GNPs did not change. However, water evaporates during lyophilization, which gradually increases the concentration of the nanoparticles and shortens the distance of the nanoparticles. Thus, the GNPs sticked together to form the solid material.

We further observed the biomaterials before and after the treatment with water under a confocal microscope. The void space was significantly decreased after hydration (Fig. 3B). Consistent with this observation, the thickness of the biomaterial dramatically decreased (Fig. 3C). We also found that the biomaterial with an initial disc shape could transform into any shape of a defined mold after contacting and absorbing water (Fig. 3D). It indicates that this solid-to-hydrogel transformation is also tunable in physical shape and geometry. This characteristic differentiates this nanoparticle-assembled biomaterial from most solid materials or hydrogels whose shapes are usually not tunable once formed.

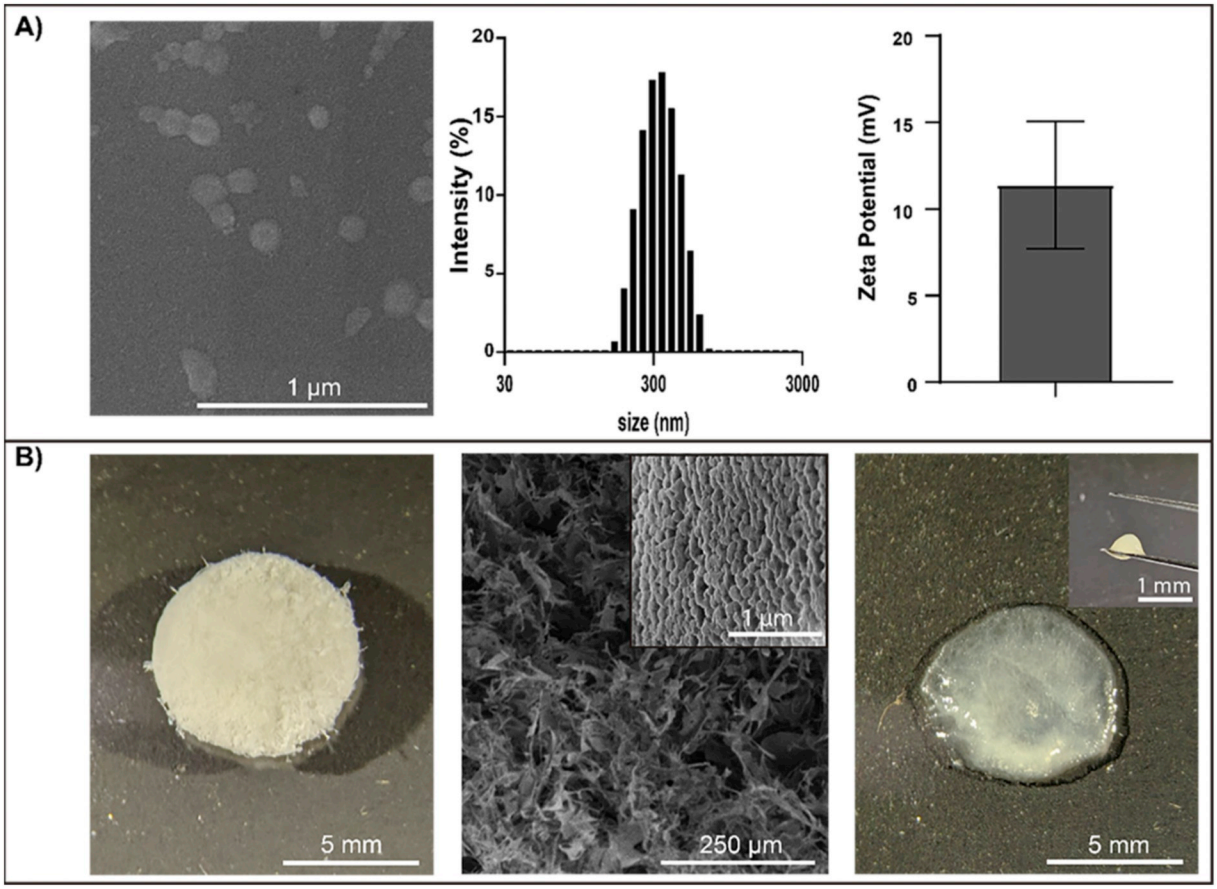

Fig. 2. Nanoparticle characterization and assembly. A) Characterization of GNPs. Left: SEM image of GNPs; Middle: size distribution of nanoparticles; Right: zeta potential. B) Formation of bulk biomaterials from GNP assembly. Left: bright-field image of nanoparticle-assembled biomaterial; Middle: SEM image of the biomaterial (the inset image shows nanoparticle aggregation). Right: bright-field image of the hydrated biomaterial (i.e., hydrogel) (the inset image shows that the hydrated biomaterial was gently picked up with a tweezer).

3.2. Synthesis of aGNPs and nanoparticle-assembled biomaterials for VEGF sequestration and release

After demonstrating that GNP-assembled biomaterials can form and have the capability of transforming into a hydrogel after hydration, we further conjugated nucleic acid aptamers onto GNPs for two reasons. First, the surface charge of the GNPs as studied above was positive. With the conjugation of nucleic acid aptamers onto GNPs, their surface could become negatively charged. This design would help understand whether negatively charged nanoparticles could also assemble to form a similar solid biomaterial. Second, nucleic acid aptamers are synthetic ligands that have high affinities and specificities against their target biomolecules similar to antibodies [34–38] Moreover, they are small in size and can be chemically synthesized [34,37]. They are also tolerant of harsh chemical and physical conditions [39]. Because of these characteristics, nucleic acid aptamers have been widely studied for biomedical applications [20,40–43]. We expected that the solid material once functionalized with aptamers would be able to sequester target biomolecules.

We used an anti-VEGF aptamer as the model to do the conjugation [44]. GNPs were modified with DBCO to provide a reaction site for azide-modified anti-VEGF aptamer. The gel image shows that the aptamer could be efficiently conjugated with GNP to form aGNPs via click chemistry (Fig. 4A). The conjugation did not lead to a significant change in size but resulted in a dramatic change of the surface charge from a positive zeta potential to a negative one (Fig. 4B). We proceeded to freeze and lyophilize the suspension of aGNPs. The image shows that, similar to GNPs, aGNPs could form a solid porous biomaterial (Fig. 4C). Moreover, this biomaterial could absorb water and form a hydrogel.

Biomaterials have been widely studied for sustained growth factor release [45–50]. Most of them are developed with the simultaneous incorporation of growth factors. However, biologics such as growth factors can easily lose their bioactivity [51–53]. Thus, it is desirable to separate the preparation and storage of biomaterials from the loading of growth factors. Our data have shown that GNP or aGNP-assembled biomaterials can absorb aqueous solutions. The preparation of these biomaterials is decoupled from the loading of a solution of growth factors. Thus, we used these GNP-assembled biomaterials to absorb the VEGF solution and examined VEGF sequestration and release. The VEGF retention increased from ~19% to ~90% in the presence of the aptamer (Fig. 5A). As the aGNP-based hydrogel can sequester VEGF, we also examined the ability of the hydrogel to control VEGF release. Within the first six hours, the aGNP- and GNP-based hydrogels released ~38% and 91% of the VEGF, respectively (Fig. 5A). After the initial release, the aGNP-based hydrogel slowly released VEGF over the next 10 days, with a daily release rate of VEGF being ~2–3%. These results suggest that the GNP-based hydrogels can release the sequestered growth factor, and that aptamers can make the release slower.

When a biomaterial is used to control the release of growth factors for an in vivo application, its working efficacy is determined not only by the amount of released growth factors but also by the bioactivity of the growth factors. Previous studies have shown that growth factors such as VEGF could lose bioactivity quickly [54]. For instance, Ekaputra et al. showed that 95% of VEGF in a hydrogel could lose their bioactivity within one week [55]. Thus, we studied the HUVEC tube formation for examining the bioactivity of the release medium with the stock VEGF

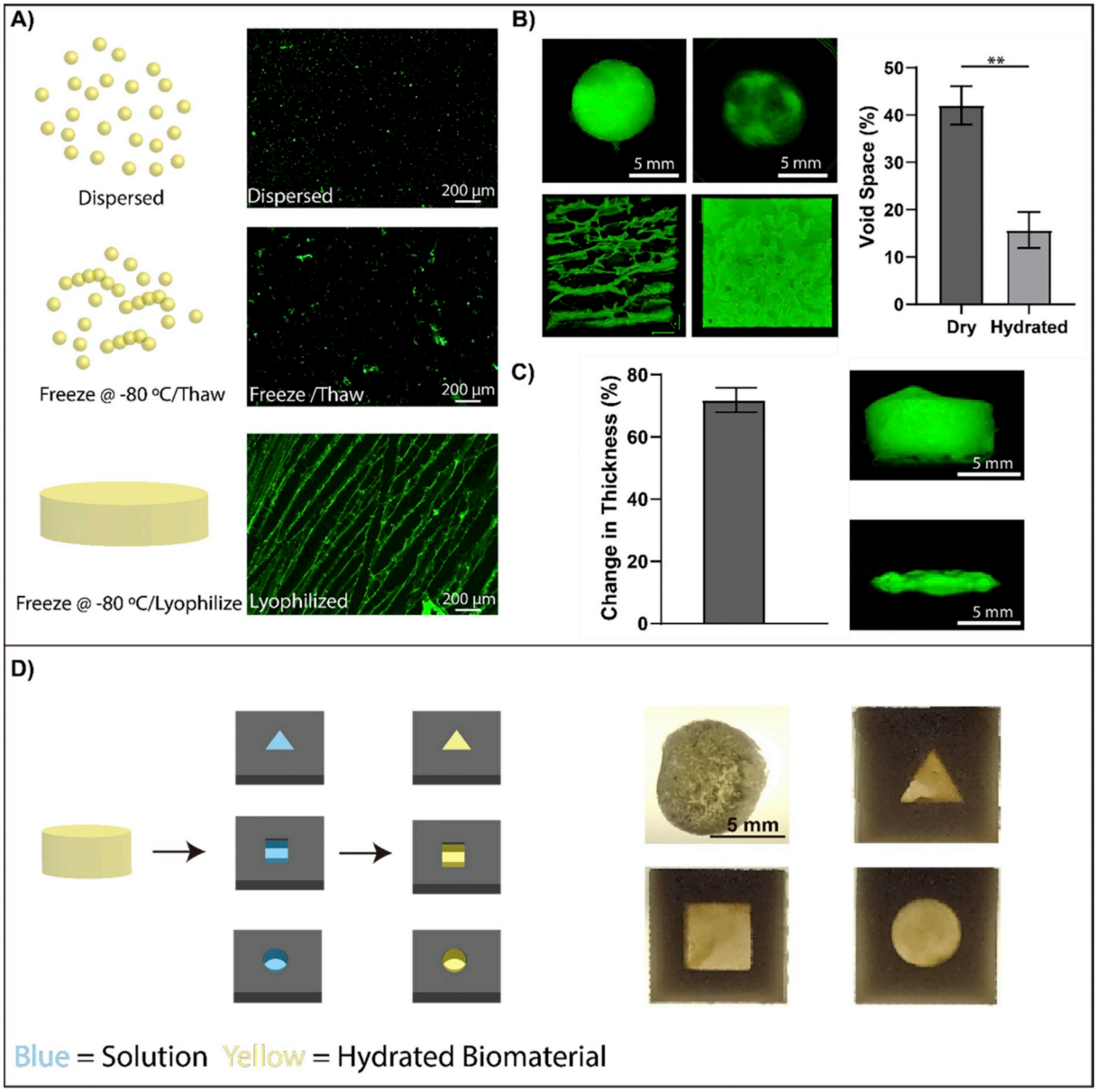

Fig. 3. Characterization of GNP-assembled biomaterials. A) Fluorescent imaging of GNPs when they were dispersed, frozen in the solution then thawed, or lyophilized. B) Images of dry and hydrated GNP-assembled biomaterials. *Z*-projections of the biomaterials examined using confocal microscopy are shown; (n = 3). **, $p < .01$. C) Quantification and fluorescent images from a side-view of the dry and hydrated biomaterials. D) Transformation of the dry disc-like biomaterial into different geometries after hydration (top view is shown).

solution as a positive control. Our data show that VEGF released from the aGNP-based hydrogel could stimulate the tube formation of HUVECs at the same level as the stock VEGF solution (Fig. 5B). It suggests that VEGF loaded in the aGNP-based hydrogel could maintain their bioactivity presumably because VEGF loading was decoupled from the procedure of preparing the biomaterials. We also found that the release medium collected from the GNP-based hydrogel stimulated minimal tube formation. The possible reasons are two-fold. One may result from the low level of released VEGF from GNP-based hydrogel as most VEGF molecules were released within the first day. The other may result from the protection of VEGF by aptamers. While aptamer-mediated VEGF binding is a physical procedure, it is similar to the form of protein immobilization that would help maintain the bioactivity of proteins [56–58].

VEGF is an important signaling molecule that can stimulate cell growth [59]. Gelatin is a biomolecule that allows for cell attachment [60–62]. As the nanoparticle-assembled biomaterials have both gelatin and VEGF, we further studied how these biomaterials affect cell proliferation using three cells including MK, HDFN and HUVEC. The cell suspension was loaded onto the biomaterials and the cells were examined on day 1 and 7. MK cells grew significantly in all three biomaterials with or without VEGF (Fig. 6A). While HDFN cells also exhibited growth, their growth in the VEGF-loaded aGNP-based hydrogel was more significant, at least in comparison to the aGNP-based hydrogel without VEGF (Fig. 6B). Interestingly, HUVECs exhibited no difference in all of the three biomaterials with or without VEGF (Fig. 6C). Moreover, the number of HUVECs decreased by day 7. However, previous studies have shown that HUVECs can grow on the surface of hydrogels loaded with VEGF. [20,61,63,64] While the exact mechanism for this decrease is unclear, we reason that this difference between the literature and this work may result from the different rigidity of biomaterials. In the literature, cells were usually cultured on standard hydrogels that allows for cell attachment and spreading. From the observation of cell morphology, HUVECs maintained a rounded

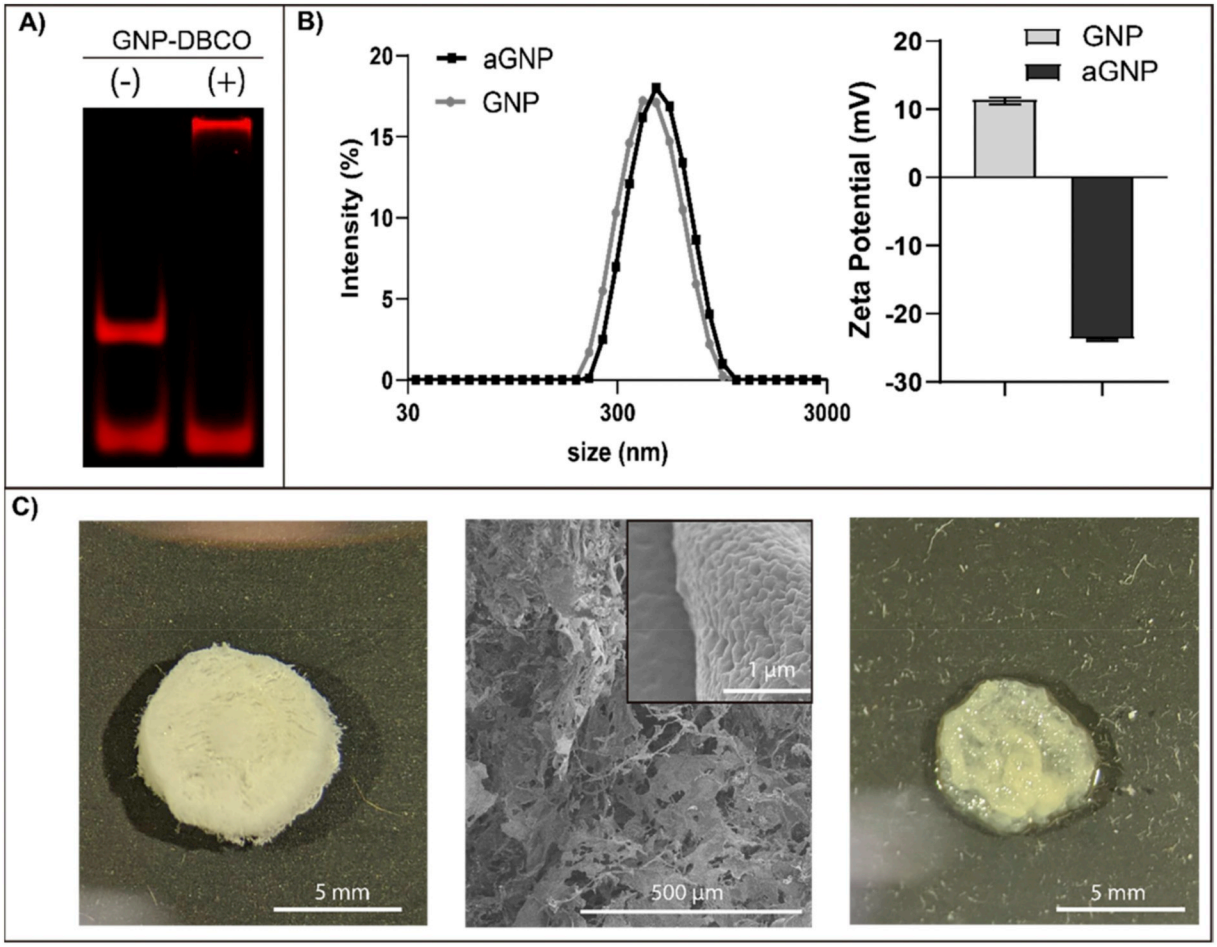

Fig. 4. Preparation of GNP-assembled biomaterials after functionalization with aptamer. A) PAGE image showing the conjugation of aptamer to GNP-DBCO. Lane 1: aptamer; lane 2: aptamer + GNP-DBCO. B) DLS and zeta potential analysis of aGNP and GNP. C) Left: bright-field image of the aGNP -assembled biomaterial; Middle: SEM image of the material (the inset figure shows nanoparticle aggregation); Right: bright-field image of the aGNP-assembled biomaterial after absorbing water.

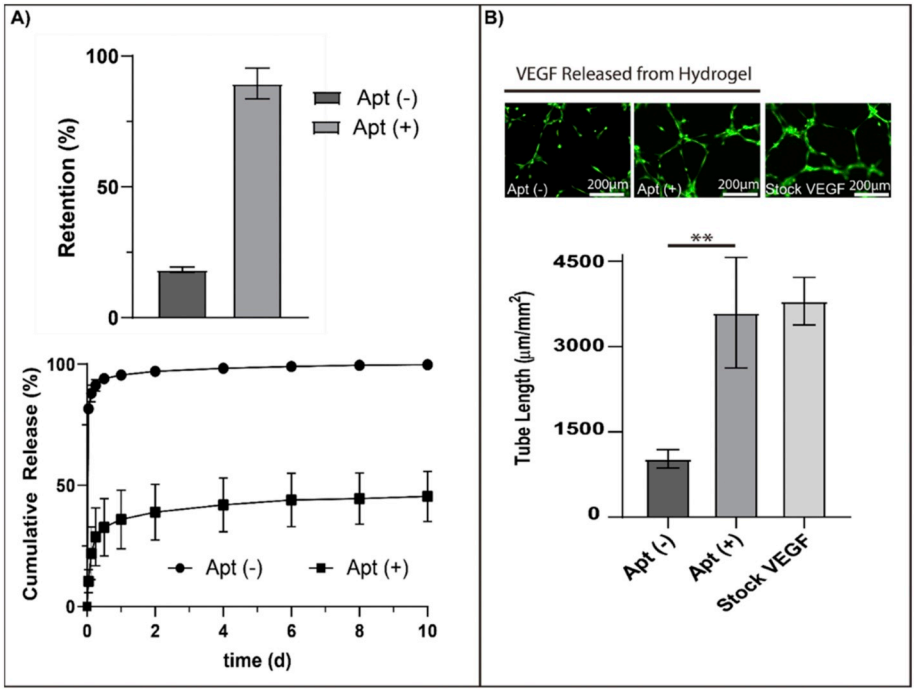

Fig. 5. VEGF retention, release, and bioactivity. A) VEGF retention and release (20:1 aptamer-to-VEGF ratio); $n = 3$. B) Tube formation examined using the HUVEC tube formation assay. Cells were stained with Calcein AM. Apt (−): release media from GNP hydrogel at day 10 (VEGF:0.4 ng/mL); Apt (+): release media from aGNP hydrogel from day 10 (VEGF:10 ng/mL); Stock VEGF (10 ng/mL). Quantitative analysis of the tube length ($n = 4$). **, $p < .01$.

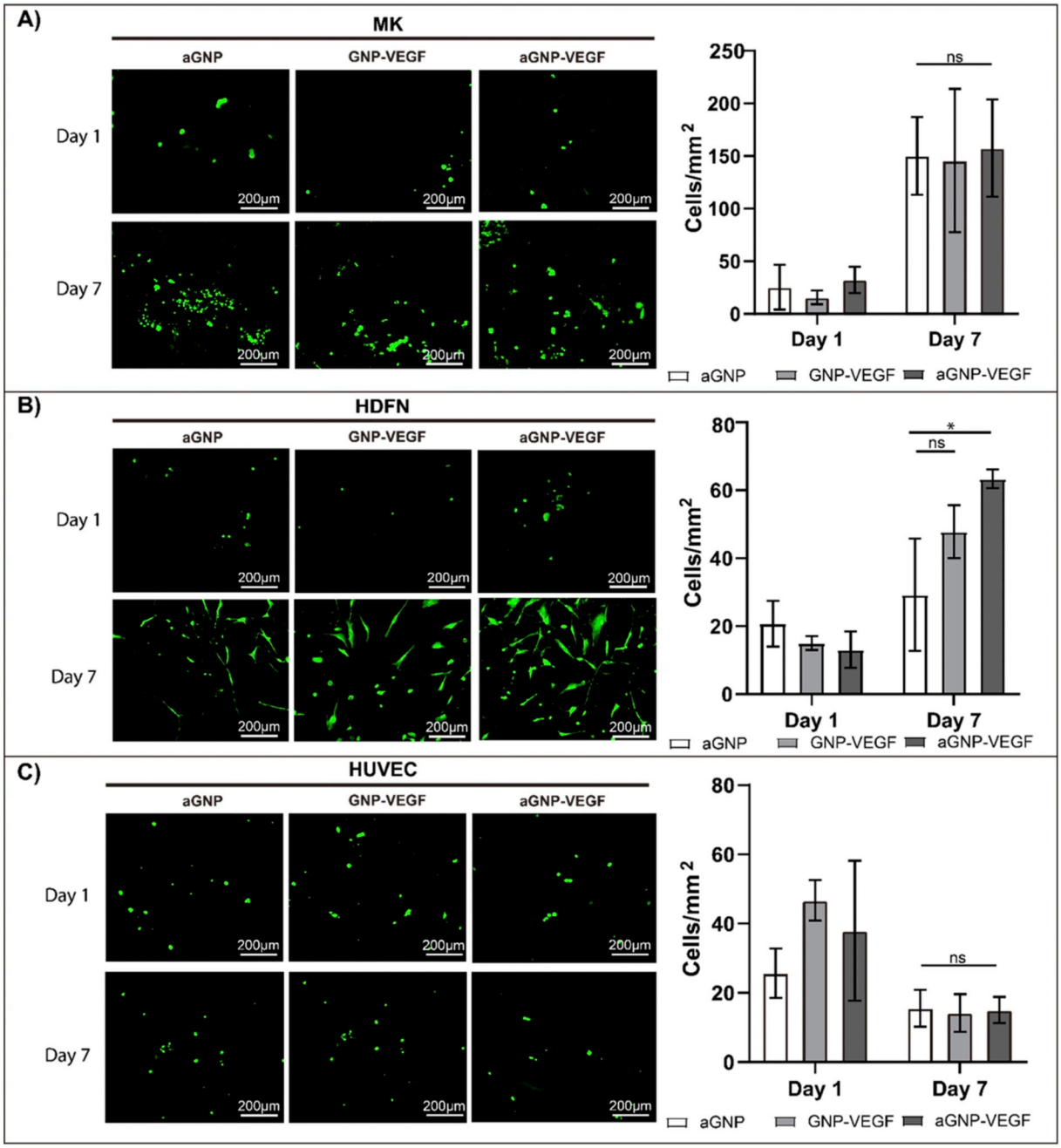

Fig. 6. Examination of cell growth on the GNP-assembled biomaterials. MK (A), HDFN (B) and HUVEC (C) were studied. The cell suspension was loaded into the GNP-assembled biomaterial and the cells were stained with Calcein AM at day 1 and 7. Left: representative images; Right: cell quantification. aGNP: aptamer functionalized nanoparticle-assembled biomaterial; GNP-VEGF: nanoparticle-assembled biomaterial with VEGF; aGNP-VEGF: aptamer functionalized nanoparticle-assembled biomaterial with VEGF. n = 3; ns, no significant difference; *, $p < .05$.

shape and did not spread in the nanoparticle-assembled hydrogels.

3.3. Implantation of nanoparticle-assembled biomaterials on the skin wound

To demonstrate potential biomedical applications of the nanoparticle-assembled biomaterials, we implanted them onto the dorsal skin wound beds and examined the skin wound healing procedure. Three biomaterials were developed for comparison, including the empty aGNP-assembled biomaterial (i.e., no VEGF loading), the VEGF-loaded aGNP-assembled biomaterial, and the VEGF-loaded GNP-assembled biomaterial. Notably, we applied the biomaterials on the wound bed and then transferred the VEGF solution onto the biomaterials, which would be similar to the procedure of a real-world application. Wounds covered with only Tegaderm were used as a control.

All three biomaterials could quickly attach onto the wound bed and gradually form transparent hydrogel films on the wound beds. The aGNP and Tegaderm groups exhibited virtually no difference throughout the course of treatment (Fig. 7A). By contrast, the wounds in both GNP-VEGF and aGNP-VEGF groups were smaller in size than the aGNP and Tegaderm groups. Statistically, the significant difference was observed on day 7, 9 and 10. Meanwhile, throughout the course of treatment, we did not see any significant difference in the promotion of wound closure between the GNP-VEGF and aGNP-VEGF groups.

To better understand the procedure of wound closure under the treatment and the difference among these groups, we harvested the

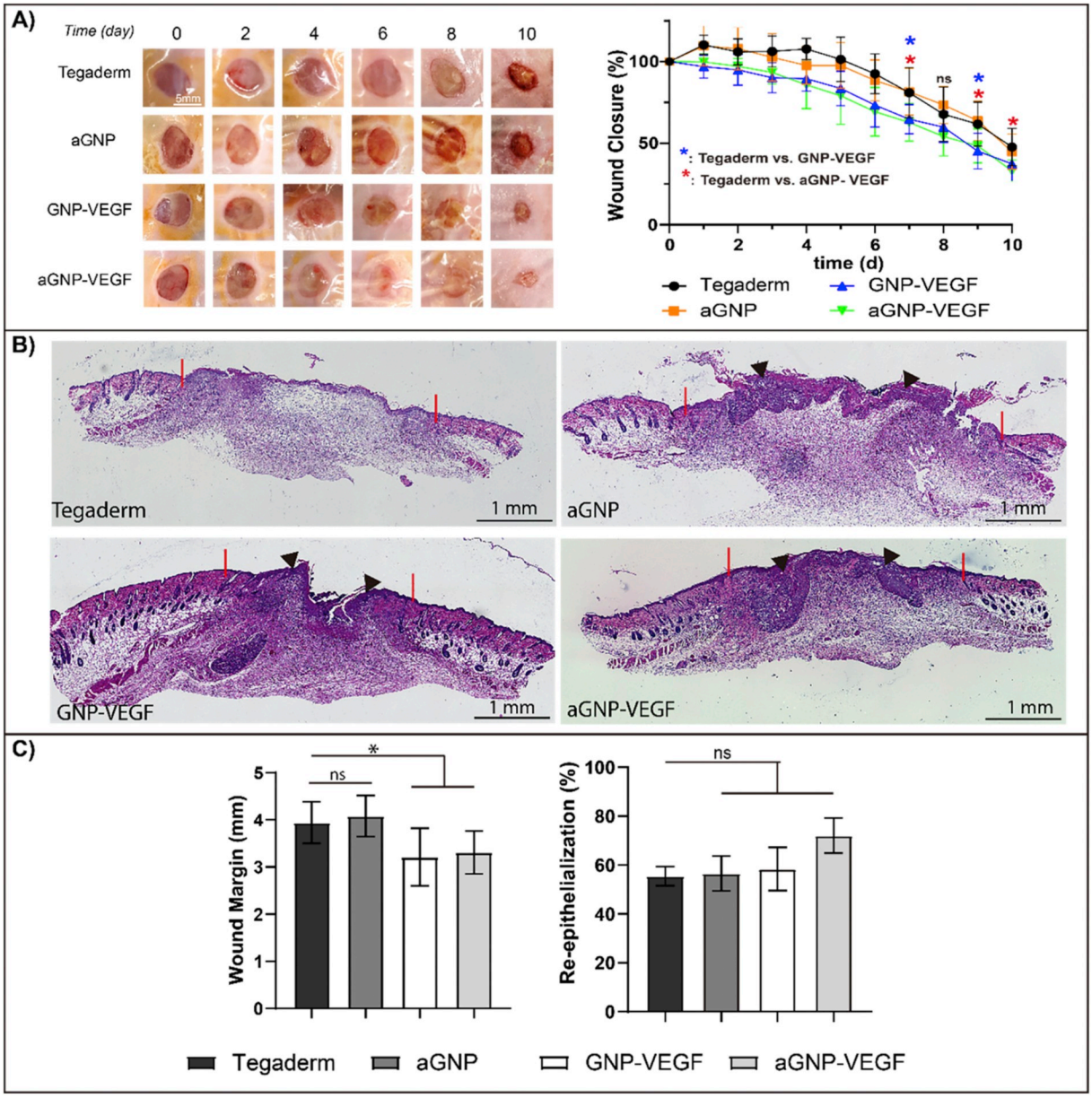

Fig. 7. GNP-assembled biomaterials for skin wound healing. A) Representative images of wounds and kinetics of wound closure. The areas of the wounds were measured and normalized by the wound size on day 0. B) H&E stained tissue collected on day 10. Black arrow heads: GNP-assembled biomaterial; Red lines: wound margins. C) Quantitative analysis of wound margin and wound re-epithelialization. $n = 8$; ns, no significant difference; *, $p < .05$. Bars indicate standard errors. (For interpretation of the references to colour in this figure legend, the reader is referred to the web version of this article.)

wound tissues at day 10 and performed tissue staining (Fig. 7B). Consistent with the macroscopic observation of wound closure, we found a shorter distance between wound margins in the GNP-VEGF and aGNP-VEGF groups than that in the aGNP and Tegaderm groups (Fig. 7C). The data also show that while the re-epithelization level in the aGNP-VEGF group was higher than the other three groups, the difference was not statistically significant.

As VEGF is an important growth factor for promoting the growth of blood vessels and has been widely used for tissue repair and wound treatment [65], we further quantified the number of blood vessels in the wound beds. The blood vessels were stained with two antibodies for CD31 and α-smooth muscle actin (α-SMA), two important biomarkers for the staining of blood vessels. The number of $CD31^+$ blood vessels in both GNP-VEGF and aGNP-VEGF groups was higher than that in the Tegaderm group (Fig. 8B). The number of $CD31^+$ and $\alpha\text{-SMA}^+$ blood vessels in both GNP-VEGF and aGNP-VEGF groups was also higher than that in the Tegaderm group (Fig. 8B). There was no significant difference between the Tegaderm and aGNP groups. These data suggest that VEGF loaded into the nanoparticle-assembled biomaterials could stimulate the growth of blood vessels.

However, the small difference between the GNP-VEGF and aGNP-VEGF groups seems inconsistent with the in vitro release data as shown in Fig. 4A. Moreover, the data published in the literature all suggest that sustained VEGF release would promote wound closure more effectively [20,66,67]. This discrepancy may be attributed to two possibilities. The first possibility is the difference of biomaterials used in different studies. As shown in the literature, the entire hydrogel was chemically crosslinked as a wound dressing for the promotion of wound closure [68–71]. In this work, while gelatin was chemically crosslinked to form GNPs, GNPs were physically assembled to form the wound dressing. The second possibility may be the difference of release kinetics in vitro and in vivo. In the in vitro study (Fig. 4A), the hydrogels

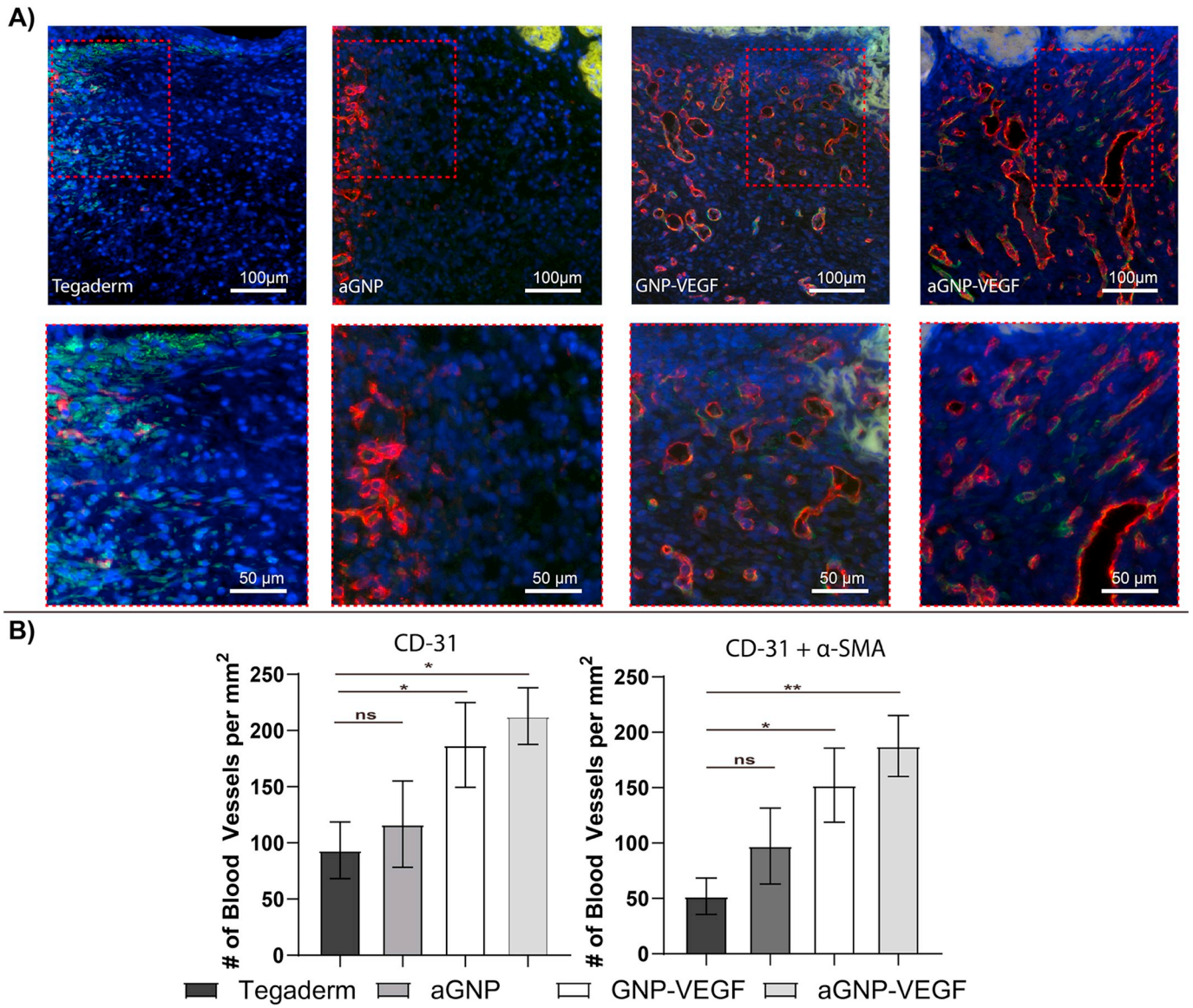

Fig. 8. Examination of angiogenesis. A) Fluorescent images of the wound bed in stained tissue sections. Red: CD-31$^+$; Green: α-SMA; Blue: DAPI. B) Quantitative analysis of the blood vessel number. Left: CD-31$^+$ blood vessels were counted; Right: co-localized CD-31$^+$ and α-SMA$^+$ blood vessels were counted. n = 8; ns, no significant difference; *, $p < .05$; **, $p < .01$. Bars indicate standard errors. (For interpretation of the references to colour in this figure legend, the reader is referred to the web version of this article.)

were fully incubated in nearly an ideal sink (i.e., the fact that the hydrogel was fully incubated in a large amount of release medium). In an in vivo environment, the top side of the hydrogel was not in contact with a bodily fluid. Moreover, the wound bed may behave as a release barrier in comparison to an open release medium. Thus, the release kinetics in vivo may be slower. To partially test this possibility, we also transferred the biomaterials into a transwell insert (Fig. S5) to do the release test. The results show that both GNP-based and aGNP-based hydrogels could release VEGF more slowly than those incubated in a release medium while the aptamer could still play a role in reducing VEGF release rate. Thus, it is possible that GNP-based hydrogels could release VEGF more slowly in vivo, which benefits wound closure and/or angiogenesis during the 10-day in vivo study in this work. These two possibilities may also have a synergistic effect on wound closure and angiogenesis. While the understanding of these biological effects is not the focus of this current study, future experiments will be designed to better understand these questions.

4. Conclusions

This work has successfully demonstrated that hydrogel nanoparticles can assemble to form a solid biomaterial through the procedure of freezing and lyophilization without the need of any additional conditions such as chemical crosslinking. This solid biomaterial can undergo solid-to-hydrogel transformation once contacting aqueous solutions. This transformation is tunable to match different shapes and geometries. The formed hydrogel can sequester and release growth factors. We envision that this nanoparticle-assembled solid biomaterial holds great potential for real-world applications such as drug delivery and regenerative medicine.

Funding sources

This study was in part supported by the National Institutes of Health (HL122311; AR073364) and the National Science Foundation (1911764).

Declaration of Competing Interest

There are no conflicts to declare.

Appendix A. Supplementary data

Supplementary data to this article can be found online at https://doi.org/10.1016/j.jconrel.2019.12.026.

References

[1] E.M. Ahmed, Hydrogel: preparation, characterization, and applications: a review, J. Adv. Res. 6 (2015) 105–121, https://doi.org/10.1016/j.jare.2013.07.006.

[2] C. Fan, D.A. Wang, Macroporous hydrogel scaffolds for three-dimensional cell culture and tissue engineering, Tissue Eng. - Part B Rev. 23 (2017) 451–461, https://doi.org/10.1089/ten.teb.2016.0465.

[3] N.S. Patil, J.S. Dordick, D.G. Rethwisch, Macroporous poly (sucrose acrylate) hydrogel for controlled release of macromolecules, Biomaterials. 17 (1996) 2343–2350.

[4] G. Sun, X. Zhang, Y.I. Shen, R. Sebastian, L.E. Dickinson, K. Fox-Talbot, M. Reinblatt, C. Steenbergen, J.W. Harmon, S. Gerecht, Dextran hydrogel scaffolds enhance angiogenic responses and promote complete skin regeneration during burn wound healing, Proc. Natl. Acad. Sci. U. S. A. 108 (2011) 20976–20981, https://doi.org/10.1073/pnas.1115973108.

[5] K.R. Kirker, Y. Luo, J.H. Nielson, J. Shelby, G.D. Prestwich, Glycosaminoglycan hydrogel films as bio-interactive dressings for wound healing, Biomaterials. 23 (2002) 3661–3671.

[6] M.C. Ford, J.P. Bertram, S.R. Hynes, M. Michaud, Q. Li, M. Young, S.S. Segal, J. Madri, E.B. Lavik, A macroporous hydrogel for the coculture of neural progenitor and endothelial cells to form functional vascular networks in vivo, Proc. Natl. Acad. Sci. U. S. A. 103 (2006) 2512–2517, https://doi.org/10.1073/pnas.0506020102.

[7] D.B. Volkin, C.R. Middaugh, The effect of temperature on protein structure, Stab. Protein Pharm. Part A. Chem. Phys. Pathways Protein Degrad, Plenum Press, New York, NY, 1992, pp. 215–247.

[8] J. Brange, Physical stability of proteins, pharm, Formul. Dev. Pept. Proteins. (2000) 89–112.

[9] M.C. Manning, K. Patel, R.T. Borchardt, Stability of protein pharmaceuticals, Pharm. Res. 6 (1989) 903–918, https://doi.org/10.1023/A:1015929109894.

[10] C. Goolcharran, M. Khossravi, R.T. Borchardt, Chemical pathways of peptide and protein degradation, pharm, Formul. Dev. Pept. Proteins. (2000) 70–88.

[11] H.J. Nachash, O. Okay, Formation and structure of polyacrylamide gels, J. Appl. Polym. Sci. 60 (1996) 971–979, https://doi.org/10.1002/(SICI)1097-4628(19960516)60:7<971::AID-APP7>3.0.CO;2-J.

[12] M.R. Huglin, Hydrogels in medicine and pharmacy, edited by N A. Peppas, Br. Polym. J. 21 (1989) 184, https://doi.org/10.1002/pi.4980210223.

[13] A. Cabana, A. Aït-Kadi, J. Juhász, Study of the gelation process of polyethylene oxide(a)-polypropylene oxide(b)-polyethylene oxide, copolymer (poloxamer 407) aqueous solutions, J. Colloid Interface Sci. 190 (1997) 307–312, https://doi.org/10.1006/jcis.1997.4880.

[14] Y. Tabata, Y. Ikada, Protein release from gelatin matrices, Adv. Drug Deliv. Rev. 31 (1998) 287–301, https://doi.org/10.1016/S0169-409X(97)00125-7.

[15] C.J. Coester, K. Langer, H.V. Briesen, J. Kreuter, Gelatin nanoparticles by two step desolvation - a new preparation method, surface modfications and cell uptake, J. Microencapsul. 17 (2000) 187–193, https://doi.org/10.1080/026520400288427.

[16] T.G. Shutava, S.S. Balkundi, P. Vangala, J.J. Steffan, R.L. Bigelow, J.A. Cardelli, D.P. O'Neal, Y.M. Lvov, Layer-by-layer-coated gelatin nanoparticles as a vehicle for delivery of natural polyphenols, ACS Nano 3 (2009) 1877–1885, https://doi.org/10.1021/nn900451a.

[17] H. Wang, M.B. Hansen, D.W.P.M. Löwik, J.C.M. Van Hest, Y. Li, J.A. Jansen, S.C.G. Leeuwenburgh, Oppositely Charged Gelatin Nanospheres as Building Blocks for Injectable and Biodegradable Gels, (2011), pp. 119–124, https://doi.org/10.1002/adma.201003908.

[18] S. Balthasar, K. Michaelis, N. Dinauer, H. Von Briesen, J. Kreuter, K. Langer, Preparation and characterisation of antibody modified gelatin nanoparticles as drug carrier system for uptake in lymphocytes, Biomaterials. 26 (2005) 2723–2732, https://doi.org/10.1016/j.biomaterials.2004.07.047.

[19] S. Ashikari-Hada, H. Habuchi, Y. Kariya, K. Kimata, Heparin regulates vascular endothelial growth factor165- dependent mitogenic activity, tube formation, and its receptor phosphorylation of human endothelial cells: comparison of the effects of heparin and modified heparins, J. Biol. Chem. 280 (2005) 31508–31515, https://doi.org/10.1074/jbc.M414581200.

[20] N. Zhao, J. Coyne, M. Xu, X. Zhang, A. Suzuki, P. Shi, J. Lai, G.H. Fong, N. Xiong, Y. Wang, Assembly of bifunctional aptamer-fibrinogen Macromer for VEGF delivery and skin wound healing, Chem. Mater. 31 (2019) 1006–1015, https://doi.org/10.1021/acs.chemmater.8b04486.

[21] N. Zhao, A. Suzuki, X. Zhang, P. Shi, L. Abune, J. Coyne, H. Jia, N. Xiong, G. Zhang, Y. Wang, Dual aptamer-functionalized in situ injectable fibrin hydrogel for promotion of angiogenesis via codelivery of vascular endothelial growth factor and platelet-derived growth factor-BB, ACS Appl. Mater. Interfaces 11 (2019) 18123–18132, https://doi.org/10.1021/acsami.9b02462.

[22] A.O. Elzoghby, Gelatin-based nanoparticles as drug and gene delivery systems: reviewing three decades of research, J. Control. Release 172 (2013) 1075–1091, https://doi.org/10.1016/j.jconrel.2013.09.019.

[23] Y. Zeng, L. Zhu, Q. Han, W. Liu, X. Mao, Y. Li, N. Yu, S. Feng, Q. Fu, X. Wang, Y. Du, R.C. Zhao, Preformed gelatin microcryogels as injectable cell carriers for enhanced skin wound healing, Acta Biomater. 25 (2015) 291–303, https://doi.org/10.1016/j.actbio.2015.07.042.

[24] S. Young, M. Wong, Y. Tabata, A.G. Mikos, Gelatin as a delivery vehicle for the controlled release of bioactive molecules, J. Control. Release 109 (2005) 256–274, https://doi.org/10.1016/j.jconrel.2005.09.023.

[25] J. Jiang, G. Oberdörster, P. Biswas, Characterization of size, surface charge, and agglomeration state of nanoparticle dispersions for toxicological studies, J. Nanopart. Res. 11 (2009) 77–89, https://doi.org/10.1007/s11051-008-9446-4.

[26] K.L. Chen, M. Elimelech, Influence of humic acid on the aggregation kinetics of fullerene (C60) nanoparticles in monovalent and divalent electrolyte solutions, J. Colloid Interface Sci. 309 (2007) 126–134, https://doi.org/10.1016/j.jcis.2007.01.074.

[27] J. Brant, H. Lecoanet, M. Hotze, M. Wiesner, Comparison of Electrokinetic properties of colloidal fullerenes (n-C60) formed using two procedures, Environ. Sci. Technol. 39 (2005) 6343–6351, https://doi.org/10.1021/es050090d.

[28] N. Saleh, H.J. Kim, T. Phenrat, K. Matyjaszewski, R.D. Tilton, G.V. Lowry, Ionic strength and composition affect the mobility of surface-modified Fe0 nanoparticles in water-saturated sand columns, Environ. Sci. Technol. 42 (2008) 3349–3355, https://doi.org/10.1021/es071936b.

[29] L.K. Limbach, Y. Li, R.N. Grass, T.J. Brunner, M.A. Hintermann, M. Muller, D. Gunther, W.J. Stark, Oxide nanoparticle uptake in human lung fibroblasts: effects of particle size, agglomeration and diffusion at low concentrations, Environ. Sci. Technol. 39 (2005) 9370–9376, https://doi.org/10.1021/es051043o.

[30] E.M. Hotze, T. Phenrat, G.V. Lowry, Nanoparticle aggregation: challenges to understanding transport and reactivity in the environment, J. Environ. Qual. 39 (2010) 1909–1924, https://doi.org/10.2134/jeq2009.0462.

[31] E.J.W. Verwey, Theory of the stability of lyophobic colloids, J. Phys. Colloid Chem. 51 (1947) 631–636, https://doi.org/10.1021/j150453a001.

[32] S.M. Gatica, M.W. Cole, D. Velegol, Designing van der Waals forces between nanocolloids, Nano Lett. 5 (2005) 169–173, https://doi.org/10.1021/nl048265p.

[33] B. Derjaguin, L. Landau, Theory of the stability of strongly charged lyophobic sols and of the adhesion of strongly charged particles in solutions of electrolytes, Prog. Surf. Sci. 43 (1993) 30–59, https://doi.org/10.1016/0079-6816(93)90013-L.

[34] A. Keefe, S. Pai, A. Ellington, Aptamers as therapeutics, Nat. Rev. Drug Discov. (2010) 537–550, https://doi.org/10.1146/annurev-pharmtox-010716-104558.

[35] E.W.M. Ng, D.T. Shima, P. Calias, E.T. Cunningham, D.R. Guyer, A.P. Adamis, Pegaptanib, a targeted anti-VEGF aptamer for ocular vascular disease, Nat. Rev. Drug Discov. 5 (2006) 123–132, https://doi.org/10.1038/nrd1955.

[36] P.R. Bouchard, R.M. Hutabarat, K.M. Thompson, Discovery and development of therapeutic aptamers, Annu. Rev. Pharmacol. Toxicol. 50 (2010) 237–257, https://doi.org/10.1146/annurev.pharmtox.010909.105547.

[37] E.N. Brody, L. Gold, Aptamers as therapeutic and diagnostic agents, J. Biotechnol. 74 (2000) 5–13, https://doi.org/10.1016/S1389-0352(99)00004-5.

[38] J. Zhou, J. Rossi, Aptamers as targeted therapeutics: current potential and challenges, Nat. Rev. Drug Discov. 16 (2016) 181–202, https://doi.org/10.1038/nrd.2016.199.

[39] P.E. Burmeister, S.D. Lewis, R.F. Silva, J.R. Preiss, L.R. Horwitz, P.S. Pendergrast, T.G. McCauley, J.C. Kurz, D.M. Epstein, C. Wilson, A.D. Keefe, Direct in vitro selection of a 2′-O-methyl aptamer to VEGF, Chem. Biol. 12 (2005) 25–33, https://doi.org/10.1016/j.chembiol.2004.10.017.

[40] M.R. Battig, B. Soontornworajit, Y. Wang, Programmable release of multiple protein drugs from aptamer-functionalized hydrogels via nucleic acid hybridization, J. Am. Chem. Soc. 134 (2012) 12410–12413, https://doi.org/10.1021/ja305238a.

[41] L. Abune, N. Zhao, J. Lai, B. Peterson, S. Szczesny, Y. Wang, Macroporous hydrogels for stable sequestration and sustained release of vascular endothelial growth factor and basic fibroblast growth factor using nucleic acid aptamers, ACS Biomater. Sci. Eng. 5 (2019) 2382–2390, https://doi.org/10.1021/acsbiomaterials.9b00423.

[42] X. Zhang, M.R. Battig, Y. Wang, Programmable hydrogels for the controlled release of therapeutic nucleic acid aptamers via reversible DNA hybridization, Chem. Commun. 49 (2013) 9600–9602, https://doi.org/10.1039/c3cc45594g.

[43] M.R. Battig, Y. Huang, N. Chen, Y. Wang, Aptamer-functionalized superporous hydrogels for sequestration and release of growth factors regulated via molecular recognition, Biomaterials. 35 (2014) 8040–8048, https://doi.org/10.1016/j.biomaterials.2014.06.001.

[44] L. Gold, N. Janjic, United States Patent 5,811,533, (n.d.). doi:https://doi.org/10.1016/j.scriptamat.2005.10.045.

[45] J. Burdick, M.N. Mason, A.D. Hinman, K. Thorne, K.S. Anseth, Delivery of osteoinductive growth factors from degradable PEG hydrogels influences osteoblast differentiation and mineralization, J. Control. Release 83 (2002) 53–63, https://doi.org/10.1016/S0168-3659(02)00181-5.

[46] S. Lu, K.S. Anseth, Photopolymerization of multilaminated poly (HEMA) hydrogels for controlled release, J. Control. Release 57 (1999) 291–300, https://doi.org/10.1016/s0168-3659(98)00125-4.

[47] R. Langer, D.A. Tirrell, Designing materials for biology and medicine, Nature. 428 (2004) 487–492, https://doi.org/10.1038/nature02388.

[48] N. Peppas, P. Bures, W. Leobandung, H. Ichikawa, Hydrogels in pharmaceutical formulations, Eur. J. Pharm. Biopharm. 50 (2000) 27–46, https://doi.org/10.1016/S0939-6411(00)00090-4.

[49] T.P. Richardson, M.C. Peters, A.B. Ennett, D.J. Mooney, Polymeric system for dual growth factor delivery nature biotechnology, Nat. Biotechnol. 19 (2001) 1029–1034.

[50] S.E. Sakiyama-Elbert, J. Hubbell, Development of fibrin derivatives for controlled release of heparin- binding growth factors, J. Control. Release 65 (2000) 389–402,

https://doi.org/10.1016/S0168-3659(99)00221-7.
[51] K. Lee, E.A. Silva, D.J. Mooney, Growth factor delivery-based tissue engineering: general approaches and a review of recent developments, J. R. Soc. Interface 8 (2011) 153–170, https://doi.org/10.1098/rsif.2010.0223.
[52] Z. Wang, Z. Wang, W.W. Lu, W. Zhen, D. Yang, S. Peng, Novel biomaterial strategies for controlled growth factor delivery for biomedical applications, NPG Asia Mater. 9 (2017), https://doi.org/10.1038/am.2017.171 e4350-17.
[53] R.R. Chen, D.J. Mooney, Polymeric growth factor delivery strategies for tissue engineering, Pharm. Res. 20 (2003) 1103–1112, https://doi.org/10.1023/A:1025034925152.
[54] F. Gu, R. Neufeld, B. Amsden, Sustained release of bioactive therapeutic proteins from a biodegradable elastomeric device, J. Control. Release 117 (2007) 80–89, https://doi.org/10.1016/j.jconrel.2006.09.077.
[55] A.K. Ekaputra, G.D. Prestwich, S.M. Cool, D.W. Hutmacher, The three-dimensional vascularization of growth factor-releasing hybrid scaffold of poly (ε-caprolactone)/collagen fibers and hyaluronic acid hydrogel, Biomaterials. 32 (2011) 8108–8117, https://doi.org/10.1016/j.biomaterials.2011.07.022.
[56] T. Jesionowski, J. Zdarta, B. Krajewska, Enzyme immobilization by adsorption: a review, Adsorption. 20 (2014) 801–821, https://doi.org/10.1007/s10450-014-9623-y.
[57] H.C. Jetani, A.K. Bhadra, N.K. Jain, I. Roy, Nucleic acid aptamers stabilize proteins against different types of stress conditions, J. Pharm. Sci. 103 (2014) 100–106, https://doi.org/10.1002/jps.23785.
[58] N.R. Mohamad, N.H.C. Marzuki, N.A. Buang, F. Huyop, R.A. Wahab, An overview of technologies for immobilization of enzymes and surface analysis techniques for immobilized enzymes, Biotechnol. Biotechnol. Equip. 29 (2015) 205–220, https://doi.org/10.1080/13102818.2015.1008192.
[59] L. Claesson-Welsh, VEGF receptor signal transduction – a brief update, Vasc. Pharmacol. 86 (2016) 14–17, https://doi.org/10.1016/j.vph.2016.05.011.
[60] B. Balakrishnan, M. Mohanty, P.R. Umashankar, a. Jayakrishnan, Evaluation of an in situ forming hydrogel wound dressing based on oxidized alginate and gelatin, Biomaterials. 26 (2005) 6335–6342, https://doi.org/10.1016/j.biomaterials.2005.04.012.
[61] J.W. Nichol, S.T. Koshy, H. Bae, C.M. Hwang, S. Yamanlar, A. Khademhosseini, Cell-laden microengineered gelatin methacrylate hydrogels, Biomaterials. 31 (2010) 5536–5544, https://doi.org/10.1016/j.biomaterials.2010.03.064.
[62] Y. Liu, M.B. Chan-Park, Hydrogel based on interpenetrating polymer networks of dextran and gelatin for vascular tissue engineering, Biomaterials. 30 (2009) 196–207, https://doi.org/10.1016/j.biomaterials.2008.09.041.
[63] N. Zhao, M.R. Battig, M. Xu, X. Wang, N. Xiong, Y. Wang, Development of a dual-functional hydrogel using RGD and anti-VEGF aptamer, Macromol. Biosci. 17 (2017) 1–8, https://doi.org/10.1002/mabi.201700201.
[64] B. Byambaa, N. Annabi, K. Yue, G.T. Santiago, M.M. Alvarez, W. Jia, M. Kazemzadeh-narbat, S.R. Shin, A. Tamayol, A. Khademhosseini, Bioprinted osteogenic and vasculogenic patterns for engineering 3D bone tissue, Adv Healthcare Mater 1700015 (2017) 1–15, https://doi.org/10.1002/adhm.201700015.
[65] G. Neufeld, T. Cohen, S. Gengrinovitch, Z. Poltorak, Vascular endothelial growth factor (VEGF) and its receptors, FASEB J. 13 (1999) 9–22.
[66] H. Brem, A. Kodra, M.S. Golinko, H. Entero, O. Stojadinovic, V.M. Wang, C.M. Sheahan, A.D. Weinberg, S.L.C. Woo, H.P. Ehrlich, M. Tomic-Canic, Mechanism of sustained release of vascular endothelial growth factor in accelerating experimental diabetic healing, J. Invest. Dermatol. 129 (2009) 2275–2287, https://doi.org/10.1038/jid.2009.26.
[67] U. Freudenberg, A. Zieris, K. Chwalek, M.V. Tsurkan, M.F. Maitz, P. Atallah, K.R. Levental, S.A. Eming, C. Werner, Heparin desulfation modulates VEGF release and angiogenesis in diabetic wounds, J. Control. Release 220 (2015) 79–88, https://doi.org/10.1016/j.jconrel.2015.10.028.
[68] S. Cai, Y. Liu, Z.S. Xiao, G.D. Prestwich, Injectable glycosaminoglycan hydrogels for controlled release of human basic fibroblast growth factor, Biomaterials. 26 (2005) 6054–6067, https://doi.org/10.1016/j.biomaterials.2005.03.012.
[69] Y. Liu, S. Cai, X.Z. Shu, J. Shelby, G.D. Prestwich, Release of basic fibroblast growth factor from a crosslinked glycosaminoglycan hydrogel promotes wound healing, Wound Repair Regen. 15 (2007) 245–251, https://doi.org/10.1111/j.1524-475X.2007.00211.x.
[70] Y. Tabata, S. Hijikata, Y. Ikada, Enhanced vascularization and tissue granulation by basic fibroblast growth factor impregnated in gelatin hydrogels, J. Control. Release 31 (1994) 189–199, https://doi.org/10.1016/0168-3659(94)00035-2.
[71] R.A. Peattie, E.R. Rieke, E.M. Hewett, R.J. Fisher, X.Z. Shu, G.D. Prestwich, Dual growth factor-induced angiogenesis in vivo using hyaluronan hydrogel implants, Biomaterials. 27 (2006) 1868–1875, https://doi.org/10.1016/j.biomaterials.2005.09.035.